Chronology and phenomenology of the 1982 and 2015 Wolf volcano eruptions, Galápagos Archipelago

Benjamin Bernard[1*], Michael J. Stock[2], Diego Coppola[3], Silvana Hidalgo[1], Marco Bagnardi[4,5], Sally Gibson[2], Stephen Hernandez[1], Patricio Ramón[1], Matthew Gleeson[2]

[1] Instituto Geofísico – Escuela Politécnica Nacional, Ladrón de Guevara E11-253 y Andalucía, Quito, Ecuador

[2] Department of Earth Sciences, University of Cambridge, Cambridge, CB2 3EQ, United Kingdom

[3] Dipartimento di Scienze della Terra – Università degli Studi di Torino, Via Valperga Caluso 35, 10125 – Torino, Italy

[4] COMET, School of Earth and Environment, University of Leeds, Leeds, United Kingdom

[5] Now at Jet Propulsion Laboratory, California Institute of Technology, Pasadena, CA, United States

* Corresponding author: bbernard@igepn.edu.ec

This is a non-peer reviewed preprint submitted to EarthArXiv

This article was submitted to Journal of Volcanology and Geothermal Research on 09/11/2018 (status on 14/11/2018: Under Review)

Abstract

The 1982 and 2015 eruptions are the first at Wolf volcano, Galápagos Archipelago, with eyewitness accounts and satellite imagery. Both eruptions are characterized by a rapid, intense initial phase and multiple eruptive vents leading to the formation of large ʻaʻā lava fields with scarce pāhoehoe deposits, mostly associated with the waning phases. The 1982 eruption started on 28 August from an intra-caldera vent that produced high lava fountaining, but also occurred from a radial fissure on the SE flank. This eruption lasted for at least 9 days and generated approximately 70E+6 m^3 of lava. The 2015 eruption started on 25 May from a circumferential fissure that also produced high lava fountaining and deposited reticulite scoria on the flanks of the volcano. For the first time since monitoring Galápagos eruptions, we observed cryptotephra from the 2015 eruption reaching and depositing in mainland Ecuador, 1400 km away from the source. Lava from the 2015 circumferential vents covered large areas on the SE and E flanks. On 13 June 2015 the eruption switched to an intra-caldera vent that was active until 30 June, which produced lava flows that covered most of the caldera floor. This eruption lasted 36 days and produced ~116E+6 m^3 of lava, making it one of the largest eruptions in the Galápagos since the eruption of Sierra Negra in 1979. The combination of ground-based geophysical surveillance, remote sensing, eyewitness accounts, and detailed field work allows us, for the first time, to constrain the eruptive dynamics of this

remote volcano with a day-by-day time resolution. In particular, our approach allows quantification of eruption rates, which represents critical information for understanding volcanic systems and for hazard assessment. First order rheological calculations further enable us to constrain the eruption dynamics and emplacement of the lava fields.

Keywords

Wolf volcano; eruptive chronology; lava fountaining; lava flows; eruption rate; reticulite; cryptotephra

1. Introduction

The Galápagos Archipelago (eastern Pacific Ocean) is one of the most active regions of hotspot-related volcanism in the world, along with Hawai'i (north Pacific Ocean) and La Réunion (west Indian Ocean; Simkin, 1984). The earliest reports of eruptive activity in the Galápagos date back to the 18th century but a semi-complete record is only available for the last 100 years, due to the major colonization of the Archipelago at the end of the 19th century and beginning of the 20th century (González et al., 2008; Fig. 1). During this period, the Galápagos Archipelago has experienced, on average, one eruption every two years.

Wolf (0.02°N, 91.35°W) is the northernmost volcano on Isabela Island (Fig. 2a), which is formed by the coalescence of four other active volcanoes (Cerro Azul, Sierra Negra, Alcedo, Darwin) and a fifth potentially active volcano (Ecuador). Wolf is a 1705 m-high shield volcano and has experienced 8 eruptions within the last 100 years, equivalent to Sierra Negra. Only Fernandina and Cerro Azul in Galápagos have had more eruptions over the last century, with 20 and 10 eruptive events, respectively. All of the Wolf lava flows that have been analyzed geochemically comprise compositionally-homogeneous basalt, with highly-depleted isotopic compositions similar to typical N-MORBs (Geist et al., 2005). Due to its remote location (110 km from the nearest town) and relatively low eruptive frequency since 1950, little is known about historical activity of Wolf (Geist et al., 2005). However, eyewitness accounts and satellite imagery exist for the two most recent eruptions in 1982 and 2015; these have the potential to provide significant constraints on the eruptive dynamics. This paper aims to present an extensive description of these eruptions by coupling eyewitness accounts, available geophysical data (ground-based and remote sensing), and analyses of eruptive deposits. We use satellite-borne optical, infrared and radar imagery, photogrammetric data from Unmanned Aerial Vehicle (UAV) surveys, and field measurements to map the lava fields and estimate the volume of subaerial products. Characteristics and morphology of the deposits are used to provide first order constraints on the lava rheology. To broader our understanding of Galápagos volcanic systems, we compare the inferred eruptive dynamics and the evolution of the 1982 and 2015 eruptions at Wolf with accounts of recent eruptions elsewhere in the Galápagos Archipelago.

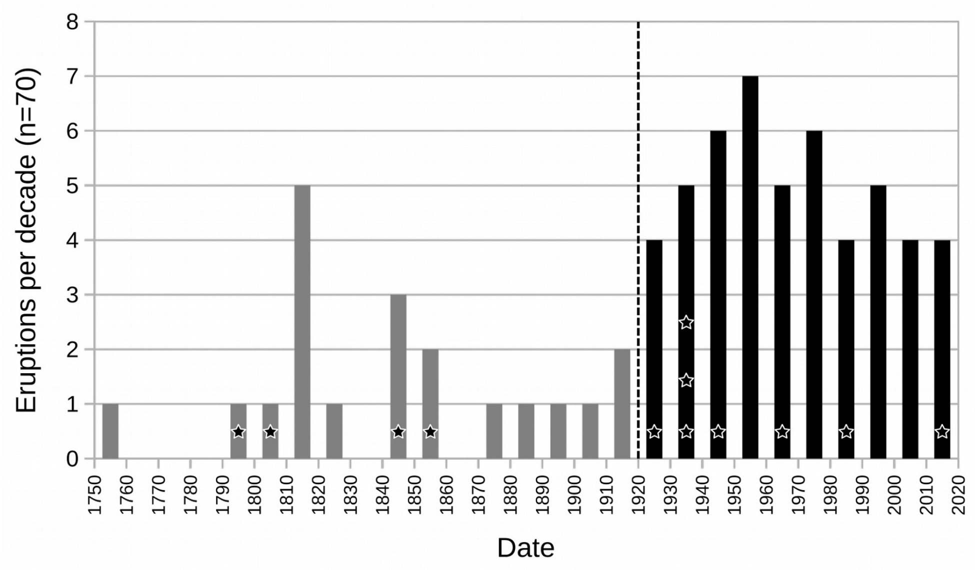

Figure 1. Eruptive frequency in the Galápagos Archipelago since 1750 (sources: modified from Global Volcanism Program, 2013). The gray series corresponds to the pre-1920 incomplete historical record (~ 1.2 eruptions/decade). The black series corresponds to the post-1920 historical record, which is considered to be relatively complete (5 eruptions/decade). The black stars with white outlines are Wolf volcano eruptions.

2. Wolf volcano

2.1. Morphology

Wolf is a large shield volcano with an inverted soup-bowl morphology characterized by gentle slopes on the lower flank and steep slopes on the upper flank, typical of other volcanoes in the western Galápagos Archipelago (Simkin and Howard, 1970). It has a rhomboidal shape (41×21 km) elongated in the NW-SE direction, and is bordered by Ecuador volcano to the west and Darwin volcano to the south (Fig. 2). The eastern, northern and south-western sides of Wolf volcano steeply dip towards the Pacific Ocean floor to a depth of ~3 km below sea level. The subaerial edifice of Wolf covers ~600 km^2 and has a volume of ~280 km^3 (Bernard and Andrade, in review). It is classified as a Type 2 Galápagos shield volcano, along with Cerro Azul and Fernandina; these have distinctly steeper slopes at intermediate elevations and deeper calderas than Type 1 volcanoes such as Sierra Negra, Alcedo and Darwin (Mouginis-Mark et al., 1996). The summit caldera is slightly elongated in the NW-SE direction (Munro and Rowland, 1996) and has an area of ~25 km^2 and a volume of ~10 km^3 (6.2×5.3 km-diameter, 700 m-deep; Bernard and Andrade, in review). The caldera hosts several benches with the largest one (3.9×0.9 km) located on the western side, ~260 m below the caldera rim. The caldera walls also exhibit landslide scars, with an associated debris avalanche deposit covering the south-east part of the caldera floor. The south-west side of the caldera is the site of two eruptive vents that were active during most of the 1982 eruption (Geist et al., 2005).

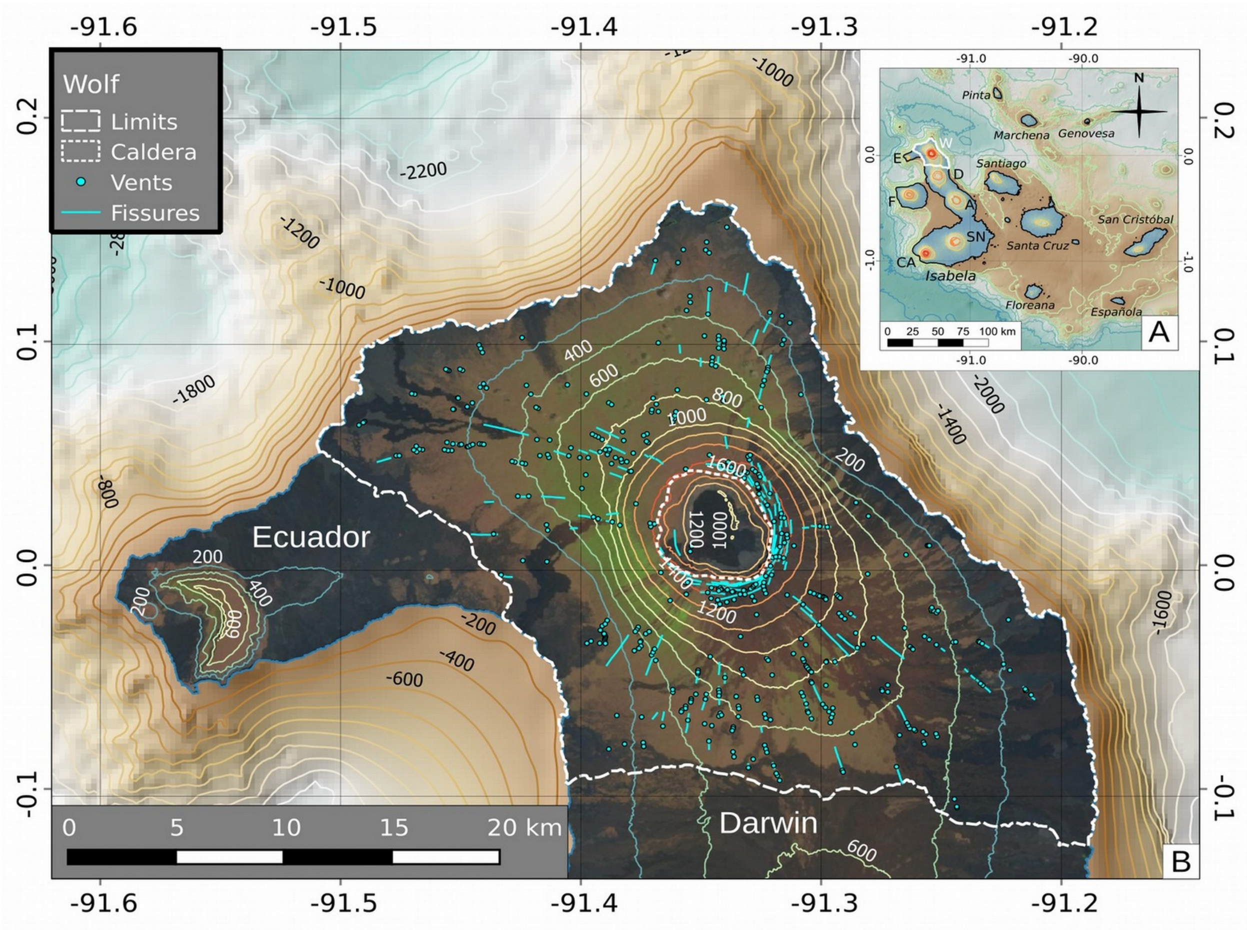

Figure 2. A) Location of Wolf volcano (W) and Isabela Island in the Galápagos Archipelago (A: Alcedo; CA: Cerro Azul, D: Darwin, E: Ecuador; F: Fernandina; SN: Sierra Negra); B) fissures and vents locations on Wolf volcano (modified from Bernard and Andrade, in review). Bathymetry: 250 m global multi-resolution topography, Ryan et al. (2009); Islands topography: JAXA 30 m digital elevation model; satellite image: Landsat 7, acquired in 2001.

2.2. Structures

The shape of Wolf volcano is largely controlled by its fissure systems (Geist et al., 2005). Eruptive vents and fissures (Fig. 2b) show clear preferential orientations, with circumferential fissures around the summit caldera and radial fissures lower on its flanks (Chadwick and Howard, 1991). The radial fissure systems form diffuse rift zones, which are much wider than the rift zones observed at Hawaiian volcanoes (Geist et al., 2005). The WNW diffuse rift zone extends past the coast-line as a NW submarine ridge towards Roca Redonda (a mostly submarine volcano). The north diffuse rift zone also continues as a submarine ridge. The south diffuse rift zone is much wider (from SW to SE) but the youngest vents have a general SE orientation. The circumferential fissures consist of arcuate fissures, typically parallel to the caldera rim. Satellite observations of the vegetation distribution suggest that, in recent times, circumferential fissures have mostly been active on the eastern and southern quadrants (Fig. 2).

Table 1: Summary of Wolf historic activity (Modified from Schatz and Schatz, 1983 and Global Volcanism Program, 2013).

Eruption start	Eruption end	Intra-caldera vent	Circumferential fissure	Radial fissure	Explosive activity	Lava flow
Aug 1797						
21 Aug 1800		X			X	X
27 Sep 1849?	27 Sep 1849?					
26 Aug 1859	29 Aug 1859					
11 Apr 1925	26 Mar 1926			ESE		X
1933?				?		X?
Feb 1935						
1938?				?		X?
Jan 1948				SE (1200 m)	X	X
Mar 1963				SE (610 m)		X
28 Aug 1982	6 Sep 1982?	SW		SE (875 m)	X	X
25 May 2015	30 Jun 2015	S	SE (1580 m) to E (1635 m)		X	X

2.3. Eruptive history

The eruptive history of Wolf volcano is poorly constrained. Based on $^{40}Ar/^{39}Ar$ dating, Geist et al. (2005) proposed that the main episode of shield growth occurred over the last 100 ky but large analytical uncertainties prohibit detailed interrogation. Cosmogenic ^{3}He exposure dating suggests that the surface of Wolf is extremely young, perhaps only a few thousand years old, and comparable to the other Galápagos volcanoes with frequent historical activity (Reynolds et al., 1995; Naumann and Geist., 2000; Kurz and Geist, 1999). Geist et al. (2005) also suggest that Wolf suffered at least 2 stages of caldera collapse, separated by a phase of caldera filling by lava flows. The surface of Wolf is mostly covered by ‘a‘ā lava deposits, with scarce pāhoehoe lava deposits. Historic activity in the last century is poorly constrained due to the remote location of the volcano but the most active area has been the SE flank, with at least 4 confirmed eruptions (Schatz and Schatz, 1983; Table 1). The

1982 and 2015 eruptions are the only ones for which eyewitness accounts, field information and remote sensing data are available (Schatz and Schatz, 1983; Global Volcanism Program, 2013; Geist et al., 2005; Bernard et al., 2015).

3. Methodology

3.1. Chronology

The chronology of the 1982 eruption at Wolf is reconstructed using the available published information and historic satellite imagery (Schatz and Schatz, 1983, Geist et al., 2005, Global Volcanism Program, 2013), while the chronology of the 2015 eruption is based on new eyewitness accounts, seismicity, field observations and satellite imagery time series (Supplementary Material 1).

In 2014 the Instituto Geofísico de la Escuela Politécnica Nacional (IG-EPN) installed a continuous seismic monitoring network in the Western Gálapagos that is composed of 6 broadband stations located on Fernandina (2), Sierra Negra (2), Cerro Azul (1) and Alcedo (1). Data from this network allow estimates of the magnitude and location of the largest events related to the 2015 eruption. To gain a better understanding of the temporal distribution of eruption-related seismicity, we apply a STA/LTA detector (short-term average/long-term average; Withers et al., 1998) to the vertical component data at the nearest station (FER1), located 35 km SW of Wolf summit, between 01 April and 31 July 2015. The majority of the detected events were either noise transients or related to seismicity at nearby Fernandina or Sierra Negra volcanoes. However, we identify ~300 events that can be related to Wolf, based on general characteristics of the waveforms, particle motions of first arrivals pointing roughly NE, and S-wave – P-wave arrival lags of approximately 6 seconds. We then submit these ~300 events to a hierarchical clustering scheme with a correlation threshold of 0.70 (Rowe et al., 2002). This results in 43 clusters from which we generate stacks to enhance signal to noise. Finally, we cross-correlate the 43 stacks across the same period as before, and identify a grand total of 465 events. This methodology provides a bird's-eye view of major trends in seismicity evolution (Fig. 4A).

We use NASA's Ozone Monitoring Instrument (OMI) to construct a time series of SO_2 outgassing throughout the eruption (e.g. McCormick et al., 2014). A mobile DOAS (Differential Optical Absorption Spectrometry) transect was performed on 29 May during a helicopter overflight to compare with the OMI time series (Fig. 4B). We then use thermal images and time series of volcanic radiative power (VRP, in Watt) during the 2015 eruption (Fig. 4C), provided by the MIROVA system (Coppola et al., 2016). In detail, following the approach of Coppola et al. (2013), we use these data sources to estimate time averaged lava discharge rate (TADR) and erupted volumes. Finally, comparison between six synthetic aperture radar (SAR) images acquired at difference stages of the eruptive activity by the European Commission's Sentinel-1 satellite, allows us to detect changes in SAR coherence and track the growth of the lava fields (e.g. Dietterich et al., 2012). The emplacement of lava flows alters the scattering properties of the ground surface, causing decorrelation of the coherence SAR images.

3.2 Mapping

The 1982 lava fields of Wolf (Fig. 5) are identified by comparing Landsat satellite images from 1978 and 1982, and mapped using the QGIS Openlayers plugin (https://github.com/sourcepole/qgis-openlayers-plugin), which provides a high resolution (0.30 m/pixel) DigitalGlobe satellite image acquired on 26 December 2014. This map is coherent with an eyewitness description of the terminal lava front and the upper fissure (Schatz and Schatz, 1983; Geist et al., 2005). We map the 2015 lava fields (Fig. 6) using a combination of diverse datasets, including: thermal and optical oblique photographs acquired during two helicopter overflights (29/05/2015 and 12/06/2015), pre-eruption optical Landsat-8 (25/12/2014) and post-eruption Sentinel-2 (21/02/2017, 20 m/pixel) satellite images, Sentinel-1 SAR coherence maps, and UAV photogrammetry data acquired during post-eruption fieldwork (3-22/06/2017; 2 subsets imaging the SE lava fronts and 3 covering the E lava fronts). This approach enables mapping of both the lava fields and associated kipukas (areas surrounded but not covered by lava flows) in great detail. All data analyses are carried out using an open-source geographic information system (QGIS; http://qgis.org).

The thicknesses of the 1982 lava fields are estimated using the 30 m/pixel Advanced Land Observation Satellite Phased Array type L-band Synthetic Aperture Radar (ALOS PALSAR) digital elevation model (DEM), acquired between 2006 and 2011 and published by the Japanese Aerospace Exploration Agency (JAXA). Lava flow thickness for the 2015 SE and E lava flows are obtained using two techniques: (1) from field measurements using a TruPulse 360 laser rangefinder by averaging 5 readings at 11 waypoints (supplementary material 2); (2) using topographic profiles extracted from high resolution (~0.03 m/pixel) digital surface models (DSM) (Fig. 7, supplementary material 2). Using the ALOS PALSAR DEM and QGIS zonal statistics plugin, it was possible to calculate the volume required to inundate the caldera floor, thus reproducing the 2015 intra-caldera lava field area.

3.3 Scoria and cryptotephra characterization

Calculating the density and porosity of scoria associated with explosive activity and lava fountaining during the 2015 eruption was not possible using classical techniques, such as paraffin coating and measurements using Archimedes' principle, due to the extreme fragility of the samples. We instead calculate the volume of an ellipsoidal envelope of the size of the 3 major axes of the clasts and estimate the scoria volume using the ellipsoidal envelope volume and a correction factor for the linear relationship between ellipsoid and measured volume of 1700 pyroclasts (Supplementary material 3). The scattering of the linear relationship, expressed as two standard deviations, is then used as an error estimate. The scoria mass is measured on a 10^{-2} g resolution electronic scale to determine its density. The scoria porosity is calculated using a grain density obtained by water pycnometry on scoria powder, milled with an automatic agate mortar.

Cryptotephra was collected on 11 June in Quito in a homemade ashmeter (Bernard, 2013) that was installed on the roof of the IGEPN in anticipation of the Cotopaxi unrest. The ashmeter allows the collection of sub-millimeter deposits of ash with low ambient contamination or reworking. The cryptotephra was compared to the scoria found on Wolf volcano using an Olympus SZ61 binocular microscope.

4. Chronology of the Wolf eruptions

4.1. The 1982 eruption

There is no information regarding possible unrest before the 1982 eruption at Wolf volcano, due to the absence of a monitoring system in the Galápagos Archipelago at this time. The eruption started on 28 August 1982 with a low altitude gas plume (~4 km), which was first detected by satellite images between 13h00 and 14h00 LT (local time = Universal Time Coordinated UTC – 6; Global Volcanism Program, 2013). The first eyewitness account was made at 16h45 LT by the captain of the *La Encantada* cruise ship (Schatz and Schatz, 1983). The eruption was characterized by two main vents: one inside the caldera, which was observed first, and one on the SE flank, observed on the second day. According to estimates from the Nimbus-7 TOMS satellite, the eruption produced 1.08E+9 kg of SO_2 on 29 August (Global Volcanism Program, 2013). Schatz and Schatz (1983) describe the lava flow from the SE flank as a typical 'a'ā flow, ~200 m-wide, flowing at only 0.5-1 m/h at the time of their visit on 30 August. They estimate the thickness to be 3–4 m at the flow margin and up to 7 m in the middle of the flow. Activity on the SE flank stopped on 1 September. According to Schatz and Schatz (1983), activity from the intra-caldera vent began on 28 August and strengthened after the end of the activity from the SE fissure. Intra-caldera activity occurred from a fissure on the SW side of the caldera floor, created a new cone, and covered ~6 km^2 of the caldera floor with >5 m thick 'a'ā flows (Geist et al., 2005). During the night of 3 September, the lava fountain from the caldera vent reached 700-800 m high (i.e. higher than the caldera rim), leaving scoria deposits on the western bench. The eruption lasted at least until 6 September, and possibly until 16 October 1982 (Schatz and Schatz, 1983).

4.2. The 2015 eruption

4.2.1. Precursory activity

As of the time of writing, as well as at the time of the 2015 eruption, no dedicated ground-based monitoring system is in place at Wolf volcano. However, interferometric synthetic aperture radar (InSAR) observations provide critical constraints on the extent and location of ground deformation prior to the 2015 eruption (Stock et al., in review). The edifice showed a total of 0.6 m inflation between 1992 to 2009, associated with a source location below the summit caldera (Bagnardi, 2014). The inflation stopped between 2009 and the end of 2010. Then routine SAR data collection stopped until shortly before the 2015 eruption (Stock et al., in review).

The majority of seismicity related to the 2015 unrest and eruption at Wolf was too small to be located by the IG-EPN Galápagos seismic array. Using the FER1 station, a total of 465 earthquakes were detected and allow a better characterization of the eruptive process. The first earthquake considered to mark the start of seismic unrest immediately preceding the eruption was detected at 08h28 LT on 24 May 2015. Subsequent earthquakes were separated on an approximately hourly timescale until 18h52 LT on 24 May, when the frequency increased to one earthquake every ~30 minutes. Then, at 23h30 LT on 24 May, the frequency increased further to one earthquake every <5 minutes. Before 23h50 LT on 24 May, the earthquakes were very small (magnitude probably ≤2) making them impossible to identify on stations other than FER1. After this time, earthquakes were detected by other stations in the array and a total of 9 events ranging in magnitude between 2.1 – 4.4 were successfully located on the NE flank of Wolf (Table 2), albeit with significantly large horizontal errors (~21 km). The earthquake at 00h58 LT was the most energetic and is thought to be associated with an explosion at the onset of the eruption (Bernard et al., 2015).

Table 2. Located seismic events during the unrest and start of the 2015 eruption of Wolf volcano. LT: Local Time = UTC – 6 hours.

Date	Hour (LT)	Latitude	Longitude	Magnitude
24 May 2015	23:50:16	0.080310	-91.309450	3.3
25 May 2015	00:06:40	0.064950	-91.306290	2.4
25 May 2015	00:09:51	0.069820	-91.306820	2.1
25 May 2015	00:16:43	0.095710	-91.310440	3.5
25 May 2015	00:20:19	0.103320	-91.294740	2.8
25 May 2015	00:21:20	0.071190	-91.321980	2.5

25 May 2015	00:33:25	0.058620	-91.308400	3.0
25 May 2015	00:58:35	0.077760	-91.327510	4.4
25 May 2015	01:16:50	0.093270	-91.302550	2.2

4.2.2. Eyewitness accounts and eruption development

Dr. David Anchundia (Charles Darwin Foundation) was monitoring Mangrove finches at Tortuga Negra beach on the west side of Isabela Island at the start of the eruption and reports that activity began between 00:30 and 00:45 LT on 25 May 2015. The group woke up after an earthquake (possibly the one recorded at 00h33 LT) and saw the volcano erupting. They recorded video footage of the eruption at 00:50 LT. In this footage the eruption is already well developed with intense lava fountaining and lava flows descending the SE flank. A very intense hot spot was first observed on Wolf volcano by the Hawai'i Institute of Geophysics and Planetology (HIGP) at 01:28 LT, based on GOES 8/10 satellite information. The eruption was also observed by a cruise ship (*La Pinta*), which was sailing off the eastern coast of the volcano and first reported the eruption at 01:29 LT (Fig. 3A). Analysis of the video footage and pictures from the eruption suggests that the initial lava fountain was 100-150 m high and was fed by a >800 m long circumferential fissure located on the upper SE flank. At 02:15 LT, the Washington Volcanic Ash Advisory Center (VAAC) reported a 10.7 km high plume moving SW. Two further plumes were reported at 03:45 LT: one at 15.2 km above sea level (a.s.l.) moving E-NE, the other at 13.7 km a.s.l. moving south. Eye-witnesses report numerous episodes of lightning within the eruptive plume.

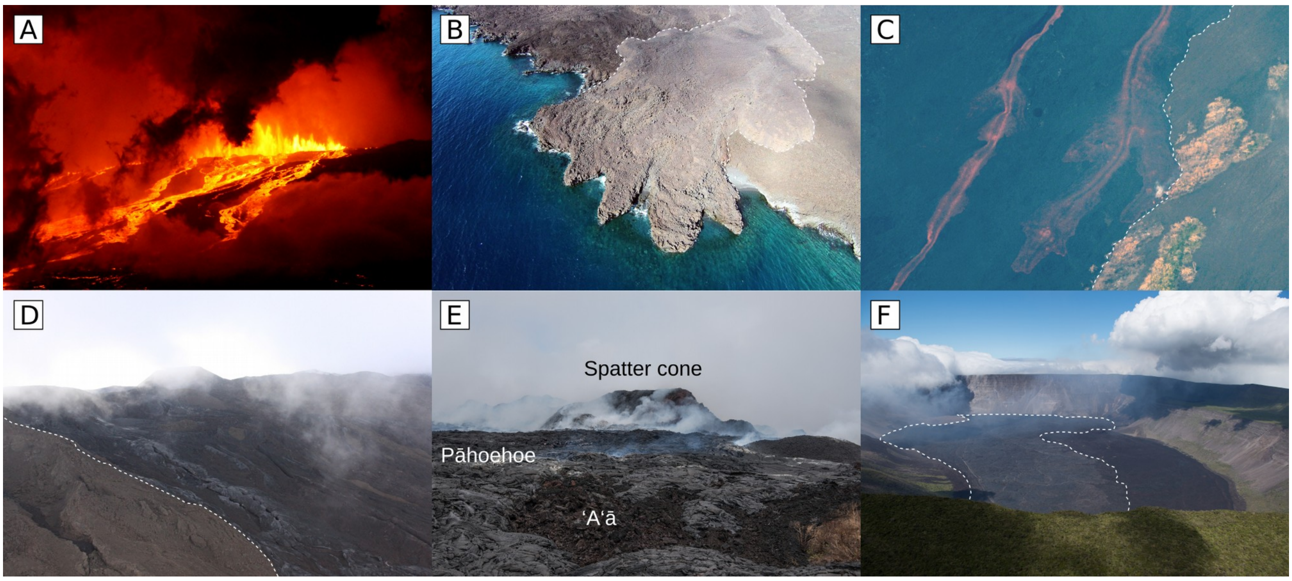

Figure 3. Photographic accounts of the 2015 eruption of Wolf volcano. A: a lava fountain from the circumferential fissure on 25 June (courtesy of the *La Pinta* crew); B: a lava delta that reached the sea between 26 and 27 June; C: active lava flows on the eastern flank on 29 June; D: a circumferential fissure still active on June 12; E: pāhoehoe and ‘a‘ā lava deposits close to the circumferential vent (courtesy of the Galápagos National Park: PNG); F: no activity was observed on 1 July and the new intra-caldera lava field (outlined by a white dashed line) is not active anymore (courtesy of the PNG).

During the first phase of the eruption (25 May – 12 June), the active vents shifted rapidly from the SE side of the outer rim of the caldera to the E side and were located along a circumferential fissure with a total length of 2.8 km. On the first day, the eruption emitted about 1.23-1.42E+8 kg of SO_2 (Fig. 4, Supplementary Material 1). Seismic activity was intense and almost continuous until 27 May, after which it decreased rapidly. According to the thermal anomalies, the peak activity for this phase occurred on 27 May (Fig. 4, Supplementary Material 1). The lava flows emitted from the E fissure probably reached the sea between 26 and 27 May (Fig. 3B). On 28 May, the gas plume extended over 3000 km and passed above mainland Ecuador. During a helicopter overflight on 29 May, IG-EPN members measured >500 °C Maximum Apparent Temperatures (MAT) at vents located at the N end of the circumferential fissure using an infrared camera, and observed active lava flows on the E flank of the volcano (Fig. 3C). The same measurements made at vents at the S end of the circumferential fissure gave temperatures of 45 °C (MAT), indicating that it was no longer active. Both SO_2 emissions and thermal anomalies slightly increased between 30 and 31 May, before decreasing rapidly. From 3 to 10 June, the eruption intensity dropped significantly. On 5 June, a Landsat-8 satellite image showed that the activity was still focused on the northern part of the circumferential fissure but limited to 5 active vents that were not producing significant lava flows. The eruption resumed on 11 June when large thermal anomalies were detected from the circumferential fissure, associated with renewed SO_2 emissions but without any significant seismic activity. The active area was about 2.2 km-long and, according to Landsat-8 imagery, mostly fed the E lava field. On 12 June, during a PNG-led field visit to assess the health of the pink iguana population on the northern side of the caldera, members of the IG-EPN noted that the E and SE lava fields were still active (Fig. 3D) and heard several explosions from circumferential vents. MAT of 86.1 °C and 96.8 °C were measured in lava flows on the SE and E flanks of the volcano, respectively. At the N end of the circumferential fissure, MAT >500 °C were measured at vents which continued to emit lava towards the E flank. IG-EPN members also observed that the caldera area was not active at that time. Pictures from a helicopter overflight by the PNG park rangers on 1 July revealed that the circumferential area was covered by both ‘a‘ā and pāhoehoe lava flows and had several new spatter and scoria cones (Fig. 3E). According to InSAR data analyses and petrological geobarometry, this first (circumferential fissure) phase of the eruption was accompanied by edifice-wide deflation due to magma extraction from a lower crustal storage region, with intra-caldera deformation suggesting associated deflation of a small shallow sill (Xu et al., 2016; Stock et al. in review).

The second phase of the 2015 eruption started on 13 June when the activity shifted to a vent within the caldera, located 2.6 km west of the circumferential fissure and 1 km east from the 1982 intra-caldera vent (Fig. 6). This intra-caldera activity is evident in the seismic record as a swarm of earthquakes from Wolf volcano started at 03h01 LT on 13 June, unfortunatly none of them was large enough to be located. After the opening of the intra-caldera vent, activity from the circumferential fissure progressively waned and was mostly over by 16 June. Thermal anomalies and SO_2 emissions indicate that the peak in activity from the caldera vent occurred on 18 June, without an obvious increase in seismic activity. Thermal energy released on June 18 was almost as high as the peak in the circumferential fissure activity on the 27 May, but the SO_2 flux was 6 times lower. The SO_2 emissions, seismicity and thermal anomalies strongly decreased until the end of June. SAR coherence maps show that the caldera lava field was still growing between 23 June and 5 July. Edifice-wide deflation measured by InSAR during the second phase of the eruption is consistent with magma extraction from the same lower crustal storage region that fed the first phase (Xu et al., 2016; Stock et al., in review). Minor thermal anomalies were detected after 30 June and are probably associated with the cooling lava fields. No SO_2 emissions were detected by satellites after 1 July. According to observations by the PNG rangers, the caldera lava field was inactive on 1 July (Fig. 3F). Hence, the eruption had mostly stopped by 30 June and had a total duration of 36 days.

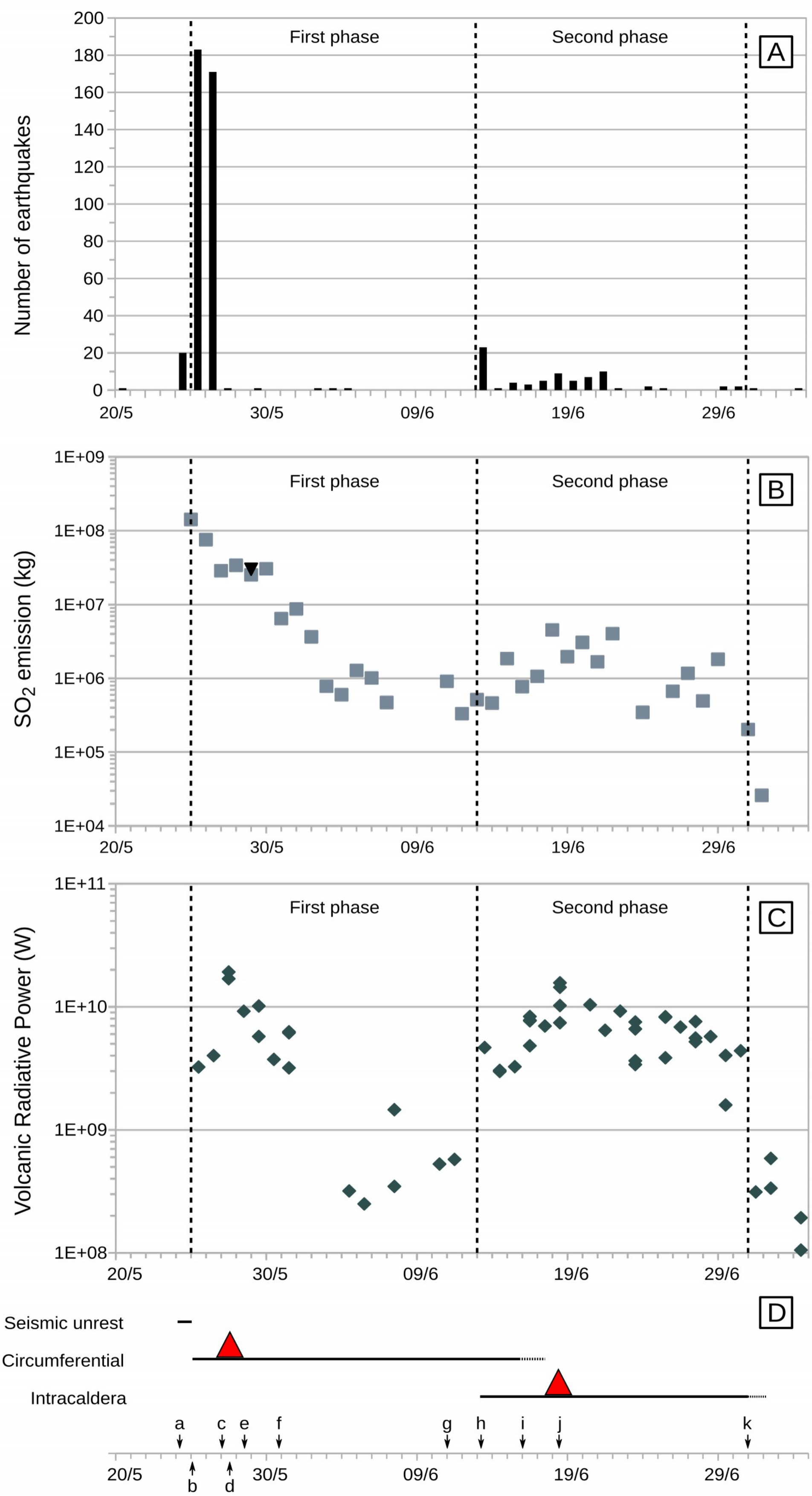

Figure 4. Evolution of the 2015 eruption of Wolf volcano. A: daily number of earthquakes detected by the FER1 broadband station. B: SO_2 emissions through time. Grey squares show emissions detected by OMI, black triangle corresponds to a mobile-DOAS flux (3.1E+7 kg/day) measurement

obtained during the helicopter overflight on 29 May. C: Volcanic Radiative Power obtained by MIROVA. D: Timeline of the eruption with main events as follows; a: seismic unrest detected at 08h28 LT on 24 May; b: eruption starts from the southern part of the circumferential fissure at ~00h33 LT on 25 May; c: lava from the E field reaches the sea between 26 and 27 May; d: first phase, highest peak of activity on 27 May according to the thermal anomalies (red triangle on the circumferential timeline); e: gas plume reaches mainland Ecuador on 28 May; f: first phase, second peak of activity between 30 and 31 May; g: renewed activity from the northern part of the circumferential fissure on 11 June; h: eruption starts from the caldera vent with seismic activity starting at 03:01 LT on 13 June; i: waning of the activity from the circumferential fissure on 16 June; j: second phase, highest peak of activity on 18 June (red triangle on the intracaldera timeline); k: waning of the activity from the caldera vent on 30 June.

5. Eruption products

5.1. 1982 Lava fields

The 1982 SE vent occurred as a 1.2 km-long radial fissure located at an elevation of 875 m and produced an ‘a‘ā lava field that reached ~250 m a.s.l. This flow is 7.2 km long, up to 1 km wide and covers an area of ~2.71 km^2, including 0.19 km^2 of kipuka (Fig. 5). The mean thickness estimated from 11 topographic profiles from the ALOS-PALSAR DEM (Fig. 5; Supplementary Material 2) along the 1982 SE lava field is 4.0 ± 1.6 m between the front of the flow and the vent area, in agreement with Schatz and Schatz (1983). From the high resolution satellite images, it appears that the 1982 intra-caldera lava field (6.16 km^2) is mainly an ‘a‘ā lava deposit with a little area of pāhoehoe lava deposit that was emplaced later during the eruption at the eastern margin. The pāhoehoe appears to be fed by lava tunnels inside the ‘a‘ā lava field and could be related to the waning phase of the eruption (between 6 September and 16 October) as it was not described by eyewitnesses on 3 September. From topographic measurements, the 1982 intra-caldera lava deposit thickness ranges 7.6-12 m, in agreement with the field estimates of Geist et al. (2005). Hence, the total volume of lava deposits produced during the 1982 eruption is 70.0 ± 23.0E+6 m^3, with 10.0 ± 4.1E+6 m^3 from the radial fissure and 60.0 ± 18.9E+6 m^3 from the caldera vent (Table 2, Supplementary Material 2). This result carries a large uncertainty because there is no accurate information on the pre-1982 caldera floor topography and because of the low resolution (30 m/pixel) of the ALOS-PALSAR DEM.

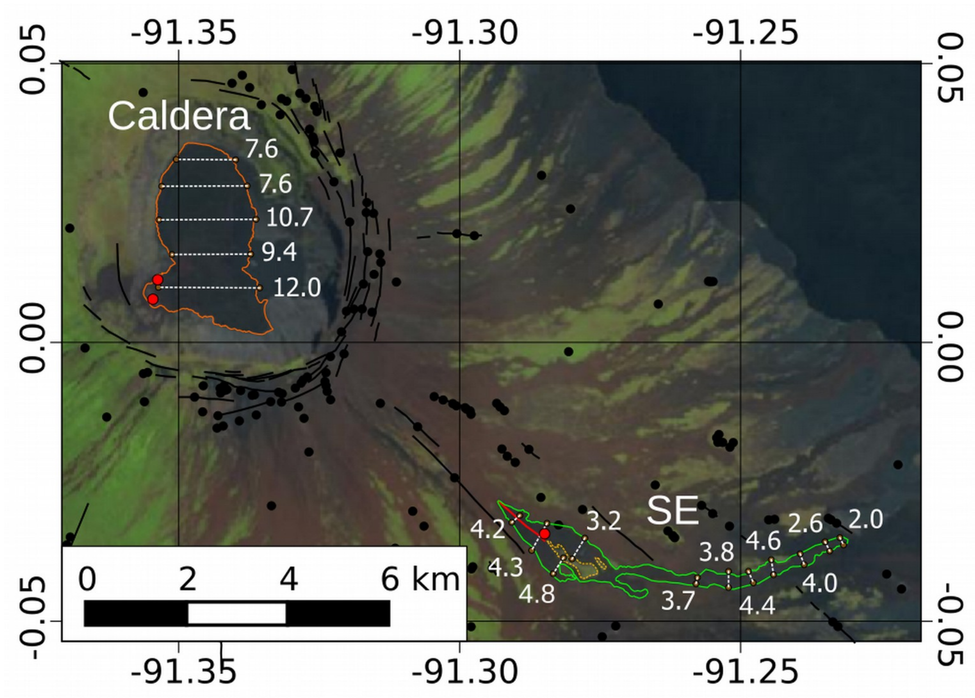

Figure 5. Distribution of lava fields and vents from the 1982 eruption of Wolf volcano. Background: Landsat image acquired on 16/05/1991; Caldera: caldera lava field; SE: southeast lava field; red dots: cones built during the eruption; red line: radial fissure; yellow dotted outlines: kipukas. Thickness values in white correspond to average thicknesses measured on the JAXA ALOS-PALSAR DEM (Supplementary Material 2).

The uncertain end date of the 1982 eruption (either 6 September or around 16 October) precludes any accurate determination of the eruption rate. However, eyewitness accounts suggest that most of the lava emissions occurred between 28 August and 6 September, giving an average eruption rate of 47.1-97.7 m^3/s (bulk deposit).

5.2. 2015 Lava fields

Lava fields associated with the 2015 eruption on Wolf cover a total subaerial area of 25.42 ± 1.17 km^2, which includes 1.43 ± 0.36 km^2 of kipukas (Fig. 6). The E lava field reached the sea but did not create a large lava delta, so we assume that the volume of the submarine lava deposit is negligible compared to the subaerial deposits. In order to estimate the average thickness of the deposits, we divided them into 7 geographically separate lava fields (Fig. 6): 1) circumferential fissure deposits (C; 2.9 km long, 400 m wide); 2) south lava field (S; 1.8 km long, up to 180 m wide); 3) south-southeast lava field (SSE: 3.7 km long, up to 500 m wide); 4) southeast lava field (SE: 10 km long, up to 2 km wide); 5) east lava field (E: 6.8 km long, up to 1.1 km wide); 6) caldera vent deposits (2.2 km long, up to 1.1 km wide; and 7) caldera floor lava field (3.5 km long, up to 1.5 km wide). The circumferential fissure (C) is the origin of the flank lava fields (S, SSE, SE and E). The activity from the caldera vent covered part of the 1982 intra-caldera lava field but also filled a depression to the east. Most of the lava flows were ‘a‘ā deposits except part of the circumferential area and possibly part of the caldera floor area, which are pāhoehoe.

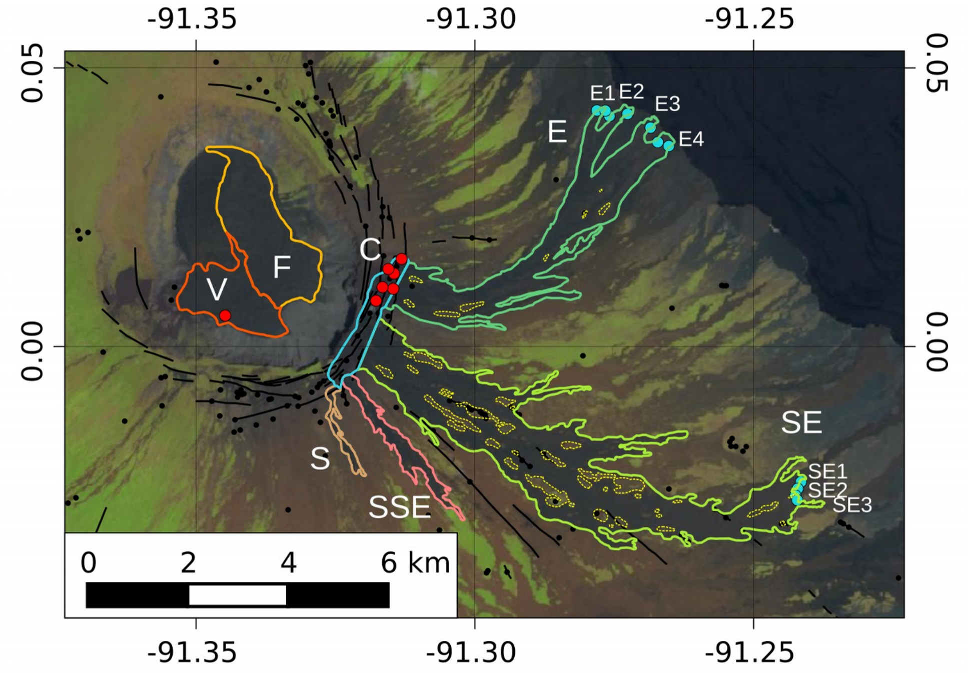

Figure 6. Distribution of lava fields and vents from the 2015 eruption of Wolf volcano. Background: Sentinel-2 image acquired on 21/02/2017; C: Circumferential fissure area; S: south lava field; SSE: south-southeast lava field; SE: southeast lava field; E: east lava field; V: caldera vent area; F: caldera floor lava field; blue dots: field thickness measurements; red dots: vents active on satellite images; yellow doted outlines: kipukas; L: lava lobes at flow front (thickness values in Supplementary Material 2).

In general, we found out that the field measurements, made on the margins of the deposits, slightly overestimate (~0.5 m) the average thickness of the lava deposits compared with the high-resolution DSM (Fig. 7, Supplementary Material 2). Profiles from the same lobe show relatively constant average thicknesses and can be used as a good approximation of the deposit thickness. The standard deviation of the thickness in each profile provides a reasonable error estimate, resulting from uncertainty in the pre-eruptive topography. Although we don’t have direct field measurements along the entire flows (i.e. upstream), we assume that the thickness would be relatively constant along the flows as observed for the 1982 SE lava field (Fig. 6). Furthermore, the slope of lower flank at lobes E1 (12°) and E2 (11°) in the E lava field, and lobe SE3 (5°) in the SE field (Fig. 6), are close to the global slope (from fissure to lava front) of their respective lava field (13.5° for the E field and 7° for the SE field). Only the lobe E3 (5°) has a slope significantly below that of the overall lava field. The average thicknesses from the SE lobes are very similar (2.4-2.7 m) while the thicknesses from the E lobes are much more variable (3.5-6.7 m). We suggest that this is related to the timing of emplacement of the different lobes. According to the SAR coherence maps, the SE lava field was emplaced before 30 May, while part of the E lava field (in particular the E1 and E2 lava lobe) was emplaced between 30 May and 11 June. To estimate the average thickness for each lava field, we used the average profile thicknesses weighted by the length of each profile. This gives an average thickness of 2.5 ± 0.8 m and 5.2 ± 1.5 m for the SE and E lava fields, respectively (Supplementary Material 2). These results are similar to other Galápagos flank eruptions, such as Fernandina 1995 (8.5 ± 2 m) and Cerro Azul 2008 (4.5 ± 2 m; Rowland et al., 2003). We assume the same average thickness for the S, SSE and SE lava field as they were emplaced during the same eruptive phase and therefore probably had a similar viscosity and discharge rate. However, due to the lack of direct measurements on the S and SSE field, we assume a conservative 50% error, slightly higher than the standard deviation on the SE lobes average thickness. In the absence of direct or DSM measurements, we estimate the thickness of the circumferential fissure area to be intermediate between the E and SE lava field with a 50% error (4.0 ± 2 m). Photographs from this area (Fig. 3E) support this approximation which is similar to the 1982 radial fissure area (4.3 ± 1.7 m).

The minimum average thickness necessary to reproduce the lava field in the caldera floor area is calculated as 7 m, with a maximum thickness in the ponding area of 17 m. These results predict a maximum 5 m thick deposit at the margins. Considering the margin thicknesses measured for the 1982 intra-caldera lava field (up to 10 m), which are similar to the margin thickness measured for the intra-caldera lava field of the 2005 eruption of Sierra Negra (Geist et al., 2008), we propose the average thickness of the caldera floor lavas to be 9.5 ± 2.5 m. In the absence of topographic constraints on the intra-caldera vent area where no ponding happened, we used the same thickness value for the caldera vent area with a conservative 50% error (average thickness of 9.5 ± 4.8 m).

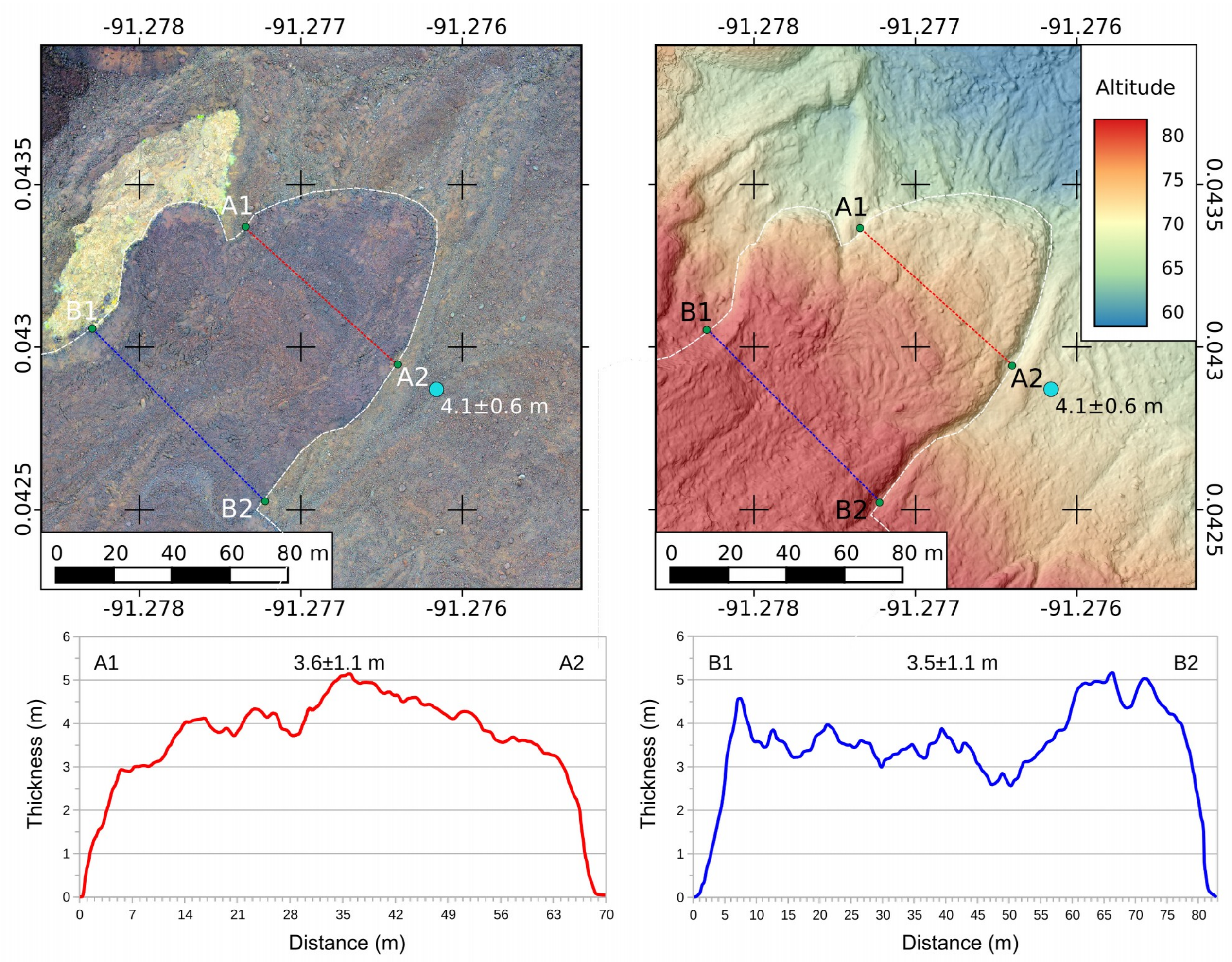

Figure 7. High resolution orthomosaic and digital surface model and corresponding topographic sections of the SE lava field lobe E1 (location in Fig. 6).

The total volume of lava deposits produced during the 2015 eruption of Wolf volcano is 116.0 ± 45.0E+6 m^3, with 63.4 ± 25.1E+6 m^3 from the first (circumferential fissure) phase and 52.6 ± 19.9E+6 m^3 from the second (caldera vent) phase. Hence, the 2015 eruption was approximately 65% larger than the 1982 eruption (Table 2). The average eruption rate for the 2015 eruption is 22.5-50.8 m^3/s (bulk deposit); this is smaller than the 1982 eruption but includes 8 days of low activity (3 to 10 June).

Based on the detailed morphology of the 2015 ‘a‘ā lava lobes it is possible to obtain some rheological constrains near flow cessation (Supplementary Material 2). Using empirical formulae (Jeffrey, 1925; Nichols, 1939), we estimated a viscosity for the SE and E lava lobes to be 3.56-4.56E+5 Pa.s and 4.17-19.7E+6 Pa.s, respectively. These values are typical of ‘a‘ā lava flows (Belousov and Belousova, 2018 and references therein). As no bulk composition difference was observed between the SE and E lava fields (M.J. Stock unpublished data), the large difference in viscosity is probably due to a combination of factors that include the slope, the discharge rate and the cooling history. Lower viscosity for the E flows is probably associated to colder lava and higher crystal content. Using the equation of Hulme (1974), the yield strength of the SE and E lava lobes is estimated in 5.23-5.56E+3 and 1.52-2.60E+4 Pa, respectively. Using the equation of Jeffrey (1925), we estimated a velocity for the SE lobe of 1.51-1.71 m/s, which compares very well with the velocity of the lava flows calculated from the thermal satellite image from 2h00 LT on 25 May, when the flow traveled 7.5 ± 1 km in about 1h30 (average velocity 1.2-1.6 m/s). The E lava lobes morphology suggests much lower velocities (0.11-0.24 m/s), consistent with the time taken for the lava flow to reach the ocean (~24 hours, average velocity 0.08 m/s).

Table 2 Summary of parameters for the 1982 and 2015 eruptions of Wolf volcano. Eruption rate values in bulk deposit (DRE = bulk*0.75 assuming 25% void).

	1982	**2015**
Flank lava field	Radial fissure (SE, ~875 m a.s.l)	Circumferential fissure (SE-E; ~1580 – ~1635 m a.s.l)
Area (without kipukas)	2.52 ± 0.14 km^2	18.46 ± 1.35 km^2
Thickness	4.0 ± 1.6 m	3.4 ± 1.4 m
Volume	10.0 ± 4.1E+6 m^3	63.4 ± 25.1E+6 m^3
Duration	3-4 days	~20 days
Average eruption rate	17.0-54.3 m^3/s	22.1-51.2 m^3/s
Caldera lava field	SW vent (~1027 m a.s.l.)	S vent (~1012 m a.s.l.)
Area	6.16 km^2 ± 0.31 km^2	5.54 km^2 ± 0.17 km^2
Thickness	9.7 ± 3.0 m	9.5 ± 3.6 m
Volume	60.0 ± 18.9E+6 m^3	52.6 ± 19.9E+6 m^3
Duration	9 days (minimum)	~18 days
Average eruption rate	52.8-101.4 m^3/s (maximum)	18.9-42.0 m^3/s
Total		
Area	8.68 ± 0.45 km^2	24.00 ± 1.52 km^2
Thickness	8.1 ± 2.9 m	4.8 ± 2.0 m
Volume	70.0 ± 23.0E+6 m^3	116.0 ± 45.0E+6 m^3
Duration	9 days (minimum)	36 days
Average eruption rate	60.4-119.5 m^3/s (maximum)	22.8-51.8 m^3/s

5.3. Reticulite and cryptotephra in Quito

On 11 June 2015, one 0.5 mm-diameter glassy fragment with a polygonal lattice was collected in an ashmeter installed on the roof of the IG-EPN, in Quito. This sample was compared with the fresh scoria found on the eastern flank of Wolf volcano during the 2017 field campaign (Fig. 8). The scoria samples have a similar glassy texture with a characteristic lattice structure typical of reticulite. The scoria bulk density ranges from 56 ± 23 to 76 ± 32 kg/m^3 and their porosity ranges from 97.3 ± 1.1 to 98.0 ± 0.8 %, using a grain density of 2782 kg/m^3 measured by water pycnometry. The grain density is consistent with the melt density (~2713 kg/m^3) at atmospheric pressure, calculated using the average glass composition (assuming near-complete degassing on ascent [<0.1 wt% H_2O] and a pre-eruptive temperature of 1150 °C; Lange and Carmichael, 1990; Stock et al., in review). Scoria was not found on top of the 2015 lava fronts, suggesting that the scoria fallout occurred before 27 May, when the east lavas arrived at the shoreline, which is consistent with the arrival of the gas plume over Ecuador (28 May). We measured the scoria size in 4 different locations and found the largest clast (10.9 cm) at 6.4 km NE of the vent, while the scoria were only 2.4-3.6 cm-diameter between 9.4 and 11 km E and SE of the vent. No ash deposits were found associated with the scoria in the field. IG-EPN operators did not observe any tephra deposits during a visit to the northern rim of the caldera on 12 June 2015. The almost complete absence of crystals in the reticulite samples allows us to use its glass composition and pre-eruptive conditions (1150 °C, Stock et al., in review) to calculate the melt viscosity (Giordano et al., 2008). The melt viscosity is ~2.3E+2 Pa.s (assuming <0.1 wt% H_2O due to efficient degassing during ascent), which is 3 to 5 order of magnitude lower than the viscosity estimated near flow cessation. Low viscosity is assumed in the formation of reticulite (1E+2 Pa.s in Mangan and Cashman, 1996). This result is consistent with the viscosity of Cerro Azul melts (2E+2 Pa.s) calculated by Naumann and Geist (2000), and could significantly reduce the uncertainty on the Cerro Azul and Fernandina effusion rates calculated by Rowland et al. (2003). Large differences between viscosity calculated by petrology and flow morphology have also been observed for Icelandic basaltic flows (Chevrel et al., 2013) and testifies the major change of viscosity that occurs when the lava reach the surface because of rapid cooling and crystallisation. Also, in this case, as well as small crystals forming in the lava as they cool, the lavas have a higher phenocryst load than the reticulite.

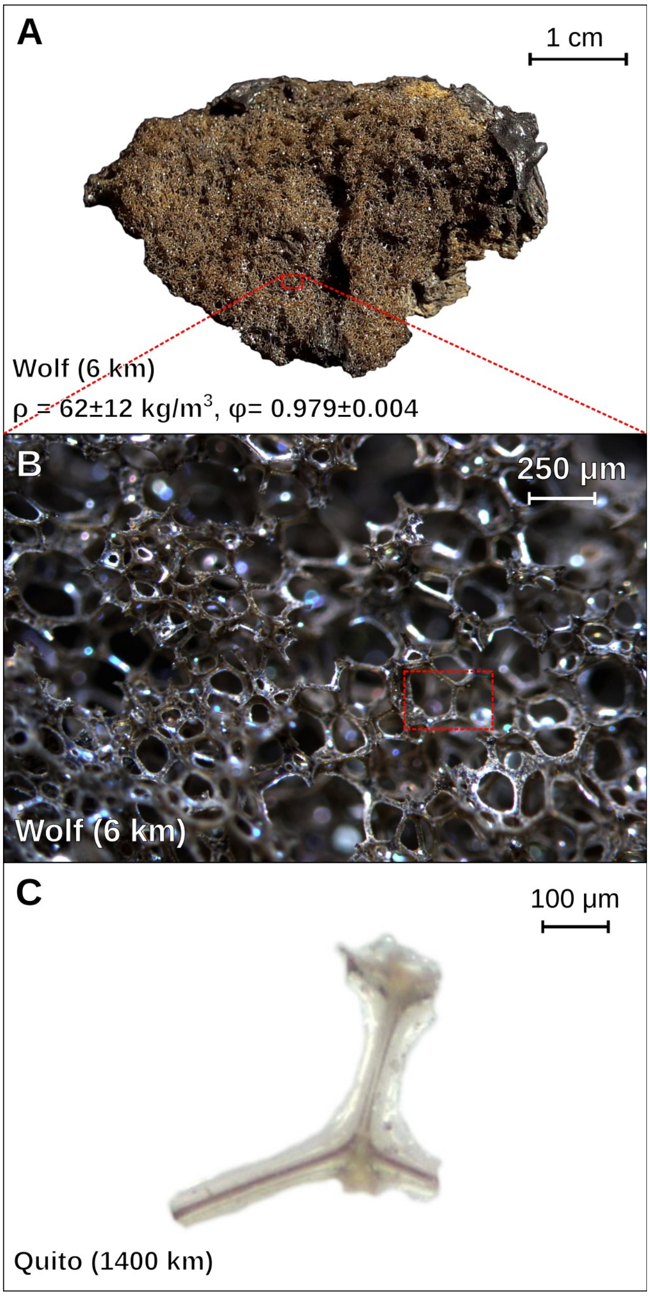

Figure 8. Glassy samples from the 2015 Wolf eruption. A) and B) Reticulite scoria found on the eastern flank of Wolf volcano. C) Cryptotephra fragment collected in Quito on 11 June 2015, 1400 km from Wolf volcano.

5.4. Time Average Discharge Rate

Using the MIROVA time series of Volcanic Radiative Power (Fig. 4) and an average melt SiO_2 content of 48.8 wt. % (Stock et al., in review), we calculated the radiant density (c_{rad}) of ~1.8E+8 J/m^3, or between ~0.9 and ~2.7E+8 J/m^3 considering the ±50% accuracy of the empirical fit (Coppola et al., 2013). Accordingly, we calculate a bulk volume of 62-186E+6 m^3, which is in excellent agreement with post-eruption field-based estimate of 71-161E+6 m^3. The comparison with field-derived volumes (Fig. 9) suggests that the two eruptive phases (circumferential and intra-caldera) were characterized by two distinct radiant densities that are likely associated with differences in topography and emplacement conditions. In detail, we found that the lava flows emplaced on the E and SE flanks of the volcano during the first phase were characterized by a radiant density at the lower boundary (~0.9E+8 J/m^3), while the lava field emplaced inside the caldera during the second phase was characterized by the radiant density at the higher boundary (~2.7E+8 J/m^3). Accordingly, the initial phase had the highest time average discharge rate (TADR) with an initial peak of 216 m^3/s (bulk deposit) on 27 May 2015 that probably corresponds to the high lava fountaining phase, which produced the reticulite tephra. Phase 2 was characterized by lower TADR that reached a maximum value of 59 m^3/s (bulk deposit) on 18 June 2015, in agreement with the much lower SO_2 emission (Fig. 4).

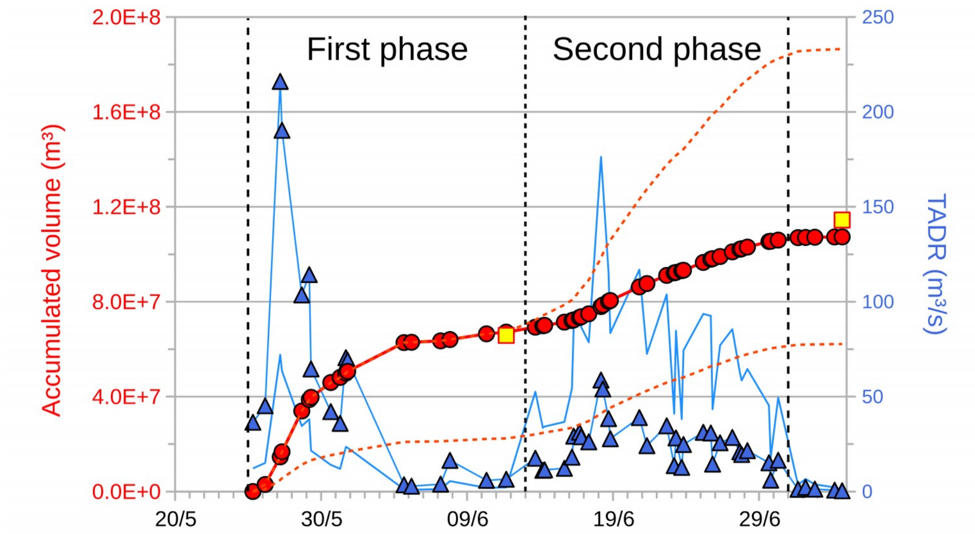

Figura 9. Accumulated volume and calculated time averaged discharge rate (TADR). Doted orange line: range of VRP-derived accumulated volume using the range of radiant densities; yellow squares: field-based accumulated volume; red circles: VRP-derived accumulated volume that best fits the field observations and SO_2 emissions; blue lines: range of time average discharge rate (TADR) using the range of radiant densities; blue triangles: TADR using the best fit to field observations and SO_2 emissions.

6. Discussion

6.1. Unrest at western Galápagos shield volcanoes

Our detailed analysis of the 1982 and 2015 Wolf eruptions provides new constrains on the eruptive dynamics of large western Galápagos shield volcanoes. The 2015 Wolf unrest is similar to recent periods of unrest at Fernandina (September 2017 and June 2018), in which a series of M2.5-4.1 earthquakes occurred over a few hours before the eruptions with only small-scale ground deformation (Vásconez et al., 2018). On the other hand, these are distinct from the recent seismic activity and large-scale ground deformation recorded at Sierra Negra before the June-August 2018 eruption. In the case of Sierra Negra, the seismic unrest lasted more than a year and included numerous M>4 earthquakes, with >5 m accumulated uplift of the caldera floor since the last eruption in 2005 (Vásconez et al., 2018). Long unrest periods at Sierra Negra, also noted in 2005 (Geist et al., 2008), could be related to larger accumulation of magma in the shallow reservoir accommodated thanks to trapdoor faulting (Jónsson et al., 2005) and evidenced by the large-scale ground deformation and large earthquakes prior to its eruptions; such unrest patterns have not yet been observed at other Galápagos volcanoes. It is worth noting that the volume withdrawn from the reservoirs calculated from InSAR during the 2015 Wolf eruption (Xu et al., 2016; Novellis et al., 2017; Stock et al. in review) are about 5 to 10 times smaller than the emitted volume, even when converting the bulk deposit volume into dense rock equivalent. Such discrepancy can be related to the role of the magma compressibility in the reservoir (Rivalta and Segall, 2008) and is consistent with most of the magma deriving directly from a deep magma storage region, as suggested by petrological barometry and the occurrence of syn-eruptive deflation of a deeper reservoir (Stock et al., in review). This process has a direct implication for hazard assessment as it suggests a major disconnect between pre-eruptive ground deformation, which is one of the main monitoring signals for remote Galápagos volcanoes, and the eruptive processes. As Fernandina unrest in 2017 and 2018 shared the same deformation characteristics as Wolf unrest in 2015, it is possible that these eruptions share similar pre-eruptive processes.

6.2. Eruption dynamics at Wolf volcano

Although reticulite has not been previously described, reports suggest that this may in fact be a common product of recent eruptions in Galápagos (Dennis Geist, pers. Com.). Such scoria are likely to break down easily due to weathering at the surface and so are unlikely to be found unless field work is done soon after an eruption. The occurrence of reticulite scoria during the 2015 Wolf eruption is evidence of the high lava fountaining (Mangan and Cashman, 1996) that was also observed during the Wolf 1982 intra-caldera activity (Schatz and Schatz, 1983; Geist et al., 2005). The reticulite scoria is associated to the high TADR at the beginning of the 2015 eruption. We note that the 1982 and 2015 Wolf eruptions are comparable, in terms of their eruptive style and intensity, to typical Hawaiian eruptions (Houghton and Gonnermann, 2008).

The average eruption rates calculated for both studied Wolf eruptions (14.2-76.1 m^3/s, dense rock equivalent = bulk*0.75) are similar to previous Galápagos eruptions at Fernandina (1988: 58 m^3/s; 2009: 27.5 m^3/s; 2017: 22.5-77.7 m^3/s; 2018: 17.4-51.8 m^3/s), Cerro Azul (1998: 17 m^3/s), and Sierra Negra (2018: 14.2-42.2 m^3/s) but are smaller than the 1979 (130 m^3/s) and 2005 (163 m^3/s)

eruptions at Sierra Negra (Rowland et al., 2003; Geist et al., 2008; Vásconez et al., 2018). Similar eruptive dynamics between Wolf, Cerro Azul and Fernandina could explain their common morphology (Mouginis-Mark et al., 1996). Geist et al. (2005) propose that the unusually steep slopes that make up the upper flank of Wolf edifice are responsible for the dominance of ‘a‘ā lava flow. However, most of the lava fields (flank and caldera) produced during the 1982 and 2015 Wolf eruptions were ‘a‘ā, irrespectively of the slope angle. Pāhoehoe flows were only confirmed on the eastern side of the caldera from the 1982 eruption and on top of the ‘a‘ā deposits close to the circumferential fissure from the 2015 eruption. From MIROVA-derived data and images from the 2015 eruption, we infer that these pāhoehoe flows close to the circumferential fissure were emplaced between 04 and 11 June, when TADR were systematically < 10 m^3/s (average 6.5 m^3/s). In contrast, ‘a’ā lavas emplaced between 25 and 31 May were characterized by average TADR of 89.8 m^3/s. Therefore, we propose that the high ‘a‘ā/pāhoehoe area ratio is caused by high eruption rates (>10 m^3/s, Rowland and Walker, 1990), and that pāhoehoe at Wolf are mostly associated with the waning phase of the eruptions. Initial activity during the 1982 and 2015 Wolf eruptions, where eruption rates are highest, are associated with significant SO_2 outgassing. This is similar to the 2005 eruption of Sierra Negra, but not other western Galapagos eruptions (i.e. at Fernandina and Cerro Azul), where the eruption rates are comparable, suggesting a decoupling between the magma volatile behavior and eruption rate.

We note that the 2015 eruption of Wolf volcano is the fourth largest Galapagos eruption since quantitative data are available (i.e. 1979), only behind Sierra Negra eruptions (1979, 2005, 2018; Vásconez et al., 2018). This might be due to the long quiescence at Wolf between the 1982 and the 2015 eruptions (33 years), which is significantly greater than typical quiescence at other active volcanoes in the western archipelago (e.g. Fernandina and Cerro Azul). Lastly, the 1982 and 2015 Wolf eruptions evolved from multiple vents, which appears to be common during moderate to large eruptions in the Galápagos (Sierra Negra 1979, 2005 and 2018; Fernandina 1995, Cerro Azul 1998). It is important to document and study such behavior in detail, as it has a direct impact on the area potentially at risk during eruptions.

7. Conclusions

Despite the remoteness of Wolf volcano, we demonstrate how eruption chronology can be reconstructed using a combination of ground-based geophysical surveillance, eyewitness accounts, remote sensing data, and post eruptive fieldwork. The 1982 and 2015 eruptions at Wolf volcano are characterized by a rapid, intense initial phase and multiple eruptive vents (SE radial fissure and caldera vent for the 1982 eruption; SE to E circumferential fissure and caldera vent for the 2015 eruption). Both eruptions showed a high lava fountaining phase, which was associated with high eruption rates and intense outgassing. We report the first detected Galápagos cryptotephra to reach continental Ecuador, which was associated with the high fountaining event in 2015. This material was transported 1400 km away from its source within a 15 km-high gas plume, carried east by stratospheric winds. The main products of the 1982 and 2015 eruptions of Wolf were large ‘a‘ā lava fields, with pāhoehoe deposits exclusively associated with the waning phase of the eruptions. The 2015 eruption was larger than the 1982 eruption and represents the fourth largest eruption in Galápagos over the last 40 years. Our new reconstruction of the chronology and phenomenology of the 1982 and 2015 Wolf eruptions provides some of the most detailed constraints on the eruptive dynamics at western Galápagos shield volcanoes to date, which is essential for volcanic surveillance, hazard assessment and contingency planning in one of the most ecologically valuable locations on Earth.

Acknowledgments

We acknowledge the logistical support of the Charles Darwin Research Station and permission of the Galápagos National Park Service, without whom this work could not have been accomplished, in particular park ranger Wilson Villamar for his assistance on the field. We also thank captain Lenin Cruz and its crew for their enthusiasm and crucial help sailing to Wolf volcano. Antonio Proaño and Francisco Vásconez (IG-EPN) help during fieldwork is also acknowledged. BB thanks the project Strengthening Resilience in Volcanic Areas (STREVA) that provided the UAV for the photogrammetric projects. BB and PR acknowledge the Secretaría de Gestión de Riesgos, Galápagos, and the Ecuadorian Navy for their logistical support with helicopter overflights. MJS acknowledges support from a Charles Darwin and Galapagos Islands Junior Research Fellowship at Christ’s College, Cambridge. MG was supported by a NERC studentship (NE/L002507/1). MB was supported the NERC Centre for the Observation and Modelling of Earthquakes, Volcanoes and Tectonics (COMET) and by an appointment to the NASA Postdoctoral Program at the Jet Propulsion Laboratory, administered by the Universities Space and Research Association (USRA) through a contract with NASA. Sentinel-1 images were derived from Copernicus SAR data obtained at https://schihub.copernicus.eu. Additional funding for fieldwork was provided by the Jeremy Willson Charitable Trust and the Mineralogical Society of Great Britain and Ireland.

References

Bagnardi, M (2014) Dynamics of Magma Supply, Storage and Migration at Basaltic Volcanoes: Geophysical Studies of the Galápagos and Hawaiian Volcanoes. Open Access Dissertations. 1179. https://scholarlyrepository.miami.edu/oa_dissertations/1179

Belousov A, Belousova M (2018) Dynamics and viscosity of ‘a’a and pahoehoe lava flows of the 2012–2013 eruption of Tolbachik volcano, Kamchatka (Russia). Bulletin of Volcanology 80:6 . doi: 10.1007/s00445-017-1180-2

Bernard B (2013) Homemade ashmeter: a low-cost, high-efficiency solution to improve tephra field-data collection for contemporary explosive eruptions. Journal of Applied Volcanology 2:1 . doi: 10.1186/2191-5040-2-1

Bernard B, Ramon P, Wright HM, Guevara A, Hidalgo S, Pacheco DA, Narváez D, Vásconez F (2015) Preliminary Results on the 2015 Eruption of Wolf Volcano, Isabela Island, Galápagos: Chronology, Dispersion of the Volcanic Products, and Insight into the Eruptive Dynamics. In: Abstract volume of the 2015 AGU Fall Meeting. San Francisco – USA

Chadwick WW, Howard KA (1991) The pattern of circumferential and radial eruptive fissures on the volcanoes of Fernandina and Isabela islands, Galapagos. Bulletin of Volcanology 53:259–275

Chevrel MO, Platz T, Hauber E, Baratoux D, Lavallée Y, Dingwell DB (2013) Lava flow rheology: A comparison of morphological and petrological methods. Earth and Planetary Science Letters 384:109–120 . doi: 10.1016/j.epsl.2013.09.022

Coppola D, Laiolo M, Cigolini C, Donne DD, Ripepe M (2016) Enhanced volcanic hot-spot detection using MODIS IR data: results from the MIROVA system. Geological Society, London, Special Publications 426:181–205 . doi: 10.1144/SP426.5

Coppola D, Laiolo M, Piscopo D, Cigolini C (2013) Rheological control on the radiant density of active lava flows and domes. Journal of Volcanology and Geothermal Research 249:39–48 . doi: 10.1016/j.jvolgeores.2012.09.005

De Novellis V, Castaldo R, De Luca C, Pepe S, Zinno I, Casu F, Lanari R, Solaro G (2017) Source modelling of the 2015 Wolf volcano (Galápagos) eruption inferred from Sentinel 1-A DInSAR deformation maps and pre-eruptive ENVISAT time series. Journal of Volcanology and Geothermal Research 344:246–256 . doi: 10.1016/j.jvolgeores.2017.05.013

Dietterich HR, Poland MP, Schmidt DA, Cashman KV, Sherrod DR, Espinosa AT (2012) Tracking lava flow emplacement on the east rift zone of Kīlauea, Hawai‘i, with synthetic aperture radar coherence. Geochemistry, Geophysics, Geosystems 13: . doi: 10.1029/2011GC004016

Geist DJ, Harpp KS, Naumann TR, Poland M, Chadwick WW, Hall M, Rader E (2008) The 2005 eruption of Sierra Negra volcano, Galápagos, Ecuador. Bulletin of Volcanology 70:655–673 . doi: 10.1007/s00445-007-0160-3

Geist DJ, Naumann TR, Standish JJ, Kurz MD, Harpp KS, White WM, Fornari DJ (2005) Wolf Volcano, Galápagos Archipelago: Melting and Magmatic Evolution at the Margins of a Mantle Plume. J Petrology 46:2197–2224. doi: 10.1093/petrology/egi052

Giordano D, Russell JK, & Dingwell DB (2008) Viscosity of Magmatic Liquids: A Model. Earth & Planetary Science Letters, 271, 123-134

Global Volcanism Program, 2013. Wolf (353020) *in* Volcanoes of the World, v. 4.7.4. Venzke, E (ed.). Smithsonian Institution. Downloaded 30 Sep 2018 (http://volcano.si.edu/volcano.cfm?vn=353020). https://doi.org/10.5479/si.GVP.VOTW4-2013

González J, Montes C, Rodríguez J, Tapia W (2008) Rethinking the Galapagos Islands as a Complex Social-Ecological System: Implications for Conservation and Management. Ecology and Society 13: . doi: 10.5751/ES-02557-130213

Houghton BF, Gonnermann HM (2008) Basaltic explosive volcanism: Constraints from deposits and models. Chemie der Erde - Geochemistry 68:117–140 . doi: 10.1016/j.chemer.2008.04.002

Hulme G (1974) The interpretation of lava flow morphology. Geophysical Journal of the Royal Astronomy Society 39:361–383

Jeffreys H (1925) The flow of water in an inclined channel of rectangular section. Philos. Mag. Ser. 6 49 (293), 793–807

Jónsson S, Zebker H, Amelung F (2005) On trapdoor faulting at Sierra Negra volcano, Galápagos. Journal of Volcanology and Geothermal Research 144:59–71 . doi: 10.1016/j.jvolgeores.2004.11.029

Kurz MD, Geist D (1999) Dynamics of the Galapagos hotspot from helium isotope geochemistry. Geochimica et Cosmochimica Acta 63:4139–4156 . doi: 10.1016/S0016-7037(99)00314-2

Lange R, Carmichael I (1990) Hydrous basaltic andesites associated with minette and related lavas in Western Mexico. Journal of Petrology 31:1225–1259

Mangan MT, Cashman KV (1996) The structure of basaltic scoria and reticulite and inferences for vesiculation, foam formation, and fragmentation in lava fountains. Journal of Volcanology and Geothermal Research 73:1–18

McCormick BT, Herzog M, Yang J, Edmonds M, Mather TA, Carn SA, Hidalgo S, Langmann B (2014) A comparison of satellite-and ground-based measurements of SO2 emissions from Tungurahua volcano, Ecuador. Journal of Geophysical Research: Atmospheres 119:4264–4285 . doi: 10.1002/2013JD019771

Mouginis-Mark PJ, Rowland SK, Garbeil H (1996) Slopes of Western Galapagos volcanoes from airborne interferometric radar. Geophys Res Lett 23:3767–3770 . doi: 10.1029/96GL03280

Munro DC, Rowland SK (1996) Caldera morphology in the western Galápagos and implications for volcano eruptive behavior and mechanisms of caldera formation. Journal of Volcanology and Geothermal Research 72:85–100. doi: 10.1016/0377-0273(95)00076-3

Naumann T, Geist D (2000) Physical volcanology and structural development of Cerro Azul Volcano, Isabela Island, Galápagos: implications for the development of Galápagos-type shield volcanoes. Bulletin of Volcanology 61:497–514. doi: 10.1007/s004450050001

Nichols RL (1939) Viscosity of lava. J. Geol. 47, 290–302.

Reynolds RW, Geist D, Kurz MD (1995) Physical volcanology and structural development of Sierra Negra volcano, Isabela Island, Galápagos archipelago. Geological Society of America Bulletin 107:1398–1410. doi: 10.1130/0016-7606(1995)107<1398:PVASDO>2.3.CO;2

Rivalta E, Segall P (2008) Magma compressibility and the missing source for some dike intrusions. Geophysical Research Letters 35: . doi: 10.1029/2007GL032521

Rowe C.A, Aster RC, Borchers B, Young CJ (2002). An automatic, adaptive algorithm for refining phase picks in large seismic data sets. Bulletin of the Seismological Society of America 92, no. 5, 1660–1674, doi: 10.1785/0120010224.

Rowland SK, Harris AJL, Wooster MJ, Amelung F, Garbeil H, Wilson L, Mouginis-Mark PJ (2003) Volumetric characteristics of lava flows from interferometric radar and multispectral satellite data: the 1995 Fernandina and 1998 Cerro Azul eruptions in the western Galápagos. Bulletin of Volcanology 65:311–330

Rowland SK, Walker GP (1990) Pahoehoe and aa in Hawaii: volumetric flow rate controls the lava structure. Bulletin of Volcanology 52:615–628

Ryan, W.B.F., S.M. Carbotte, J.O. Coplan, S. O'Hara, A. Melkonian, R. Arko, R.A. Weissel, V. Ferrini, A. Goodwillie, F. Nitsche, J. Bonczkowski, and R. Zemsky (2009), Global Multi-Resolution Topography synthesis, Geochem. Geophys. Geosyst., 10, Q03014, doi: 10.1029/2008GC002332

Schatz H, Schatz I The eruption of the volcano Wolf (Albemarle, Galápagos islands, Ecuador) in 1982—Report of eye-witnesses [in German]. Ber Nat-med Verein Innsbruck 70:17–28

Simkin T (1984) Geology of Galapagos. Biol J Linn Soc 21:61–75. doi: 10.1111/j.1095-8312.1984.tb02053.x

Simkin T, Howard K (1970) Caldera collapse in the Galapagos islands. Science 169:429–437

Vasconez FJ, Ramón P, Hernandez S, Hidalgo S, Bernard B, Ruiz M, Alvarado A, Femina PL, Ruiz G (2018) The different characteristics of the recent eruptions of Fernandina and Sierra Negra volcanoes (Galápagos, Ecuador). 1 1:127–133

Withers M, Aster R, Young C, Beiriger J, Harris M, Moore S, Trujillo J (1998) A comparison of select trigger algorithms for automated global seismic phase and event detection. Bulletin of the Seismological Society of America ; 88 (1): 95–106.

Xu W, Jónsson S, Ruch J, Aoki Y (2016) The 2015 Wolf volcano (Galápagos) eruption studied using Sentinel-1 and ALOS-2 data. Research Letter. doi: 10.1002/2016GL069820